Journal of Sedimentary Research

Journal of Sedimentary Research, 2013, v. 83, 170–182
Research Article
DOI: 10.2110/jsr.2013.12

MAGNETIC-FABRIC ANALYSIS AS A TOOL TO CONSTRAIN MECHANISMS OF DEEP-WATER MUDSTONE DEPOSITION IN THE MARNOSO ARENACEA FORMATION (MIOCENE, ITALY)

ELEONORA DALL'OLIO, FABRIZIO FELLETTI, AND GIOVANNI MUTTONI
Dipartimento di Scienze della Terra "Ardito Desio," Università degli Studi di Milano, Via Mangiagalli 34, 20133 Milano, Italy
e-mail: eleonora.dallolio@unimi.it

ABSTRACT: **Mudstone-dominated marine successions are common in the geological record, yet a full understanding of their depositional processes is often hampered by a lack of generally accepted diagnostic criteria to distinguish between hemipelagic settling and deposition from a flowing medium. The Marnoso Arenacea Formation, a turbidite unit of Miocene age cropping out in the northern Apennines of Italy, offers the possibility to address some of these uncertainties. A relatively small (~ 10%) but distinctive portion of the Marnoso Arenacea Formation is composed of white marlstone beds (WM beds) that have frequently been interpreted as due to hemipelagic settling of fine-grained particles (hemipelagites). The analysis of the anisotropy of magnetic susceptibility (AMS) revealed the presence in the WM beds of maximum susceptibility axes clustered within the depositional plane along the average paleoflow direction inferred from flute casts at the bases of the nearest turbidite beds, whereas the minimum susceptibility axes are oriented perpendicular to the bedding plane. This fabric is interpreted as largely sedimentary in origin (albeit a contribution from tectonic shortening cannot be excluded) and due to the alignment within the bedding plane of paramagnetic grains (e.g., muscovite) and possibly also ferromagnetic grains (magnetite) under low-velocity currents. The trend of the maximum susceptibility axes, and hence of the paleoflow direction, is approximately oriented NNW–SSE after correction for Apennines thrust-sheet rotation since the Miocene. These results suggest that the WM beds cannot be entirely due to hemipelagic settling, as often stated in the literature. A discussion of alternative depositional mechanisms leads us to conclude that the WM beds may have been deposited under the influence of contour currents and should therefore be referred to as muddy contourites.**

INTRODUCTION

Mudstones are a major component of marine sedimentation, and they play a fundamental role in hydrocarbon exploration and exploitation (Viana 2008). Mechanisms accountable for deep-sea mudstone accumulation include gravity-induced turbidity currents, thermohaline-induced bottom contour currents, and hemipelagic suspension settling (Rebesco and Camerlenghi 2008). Distinguishing among muddy turbidites (hemiturbidites *sensu* Stow and Wetzel 1990), contourites, and hemipelagites is not trivial (Stow and Faugères 2008; Mulder et al. 2008; Mulder et al. 2009) inasmuch as these deposits share similar sedimentological features (Stow and Wetzel 1990). The distinction is further hampered by interaction processes whereby bottom currents may incorporate and redistribute particles originated from hemipelagic–pelagic settling (Stow et al. 1998); for example, Reeder et al. (2002) and Dennielou (1997) interpreted the Sicily Channel and North Atlantic deposits, respectively, as the result of bottom-current lofting and resuspension of hemipelagic muds.

The Miocene Marnoso Arenacea turbidite system of the northern Apennines, Italy, provides the opportunity to address uncertainties concerning mechanisms of mudstone deposition in the deep sea. In the Marnoso Arenacea, distinctive white marlstone beds (hereafter WM beds) overlie mudstone layers derived from the deposition of the tails of turbidity currents (Bouma's T_e divisions). Several authors (Mutti and Ricci Lucchi 1972, 1975; Mutti 1977, 1979; Mutti and Johns 1979; Talling et al. 2007) referred to the WM beds as hemipelagites, often using the term "hemipelagic" with reference to composition rather than to a specific depositional process. Mutti and Ricci Lucchi (1972) contemplated three plausible genetic processes to account for the WM beds associated with deep-water turbidites: turbidity currents, intermediate currents (i.e., bottom currents), and "normal" settling from standing water. Later, Mutti et al. (2002) and Muzzi Magalhaes and Tinterri (2010) suggested that the WM beds could have been derived from the settling of suspension clouds produced from fading turbidity currents (hemiturbidites *sensu* Stow and Wetzel 1990).

It is therefore fair to say that despite an ever-growing body of knowledge regarding the sedimentology and depositional characteristics of the WM beds, the issue of their origin is virtually unsolved. This is reminiscent of uncertainties regarding the origin of similar white marlstone deposits from other well-studied sedimentary basins worldwide (Kuenen 1964; Van der Lingen 1969; Hesse 1975; Rupke 1975; Stow and Piper 1984; Stanley 1988; Stow and Wetzel 1990; Stow and Tabrez 1998; Mutti et al. 2002; Remacha et. al. 2005; Stow and Faugères 2008; Mulder et al. 2008; Rebesco and Camerlenghi 2008). An ultimate understanding of the sedimentary processes responsible for the deposition of the WM beds of the Marnoso Arenacea Formation, as well as of similar sediments deposited elsewhere, is hampered by conflicting interpretations on the origin of the sedimentary structures that they contain (Stow and Faugères 2008; Mulder et al. 2008).

In this paper, we attempt to decipher the origin of the WM beds by integrating sedimentological observations with study of the anisotropy of

Published Online: February 2013
 1527-1404/13/170-182/$03.00

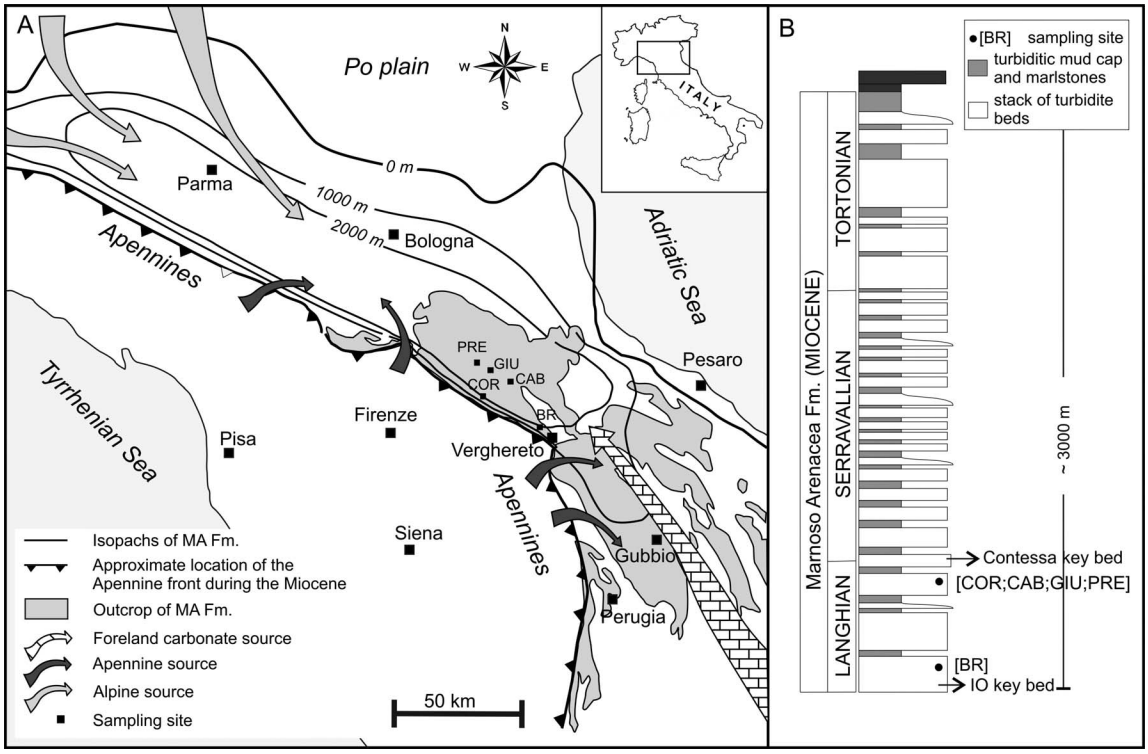

FIG. 1.—**A)** Map showing the outcrop area and thickness of the Marnoso Arenacea Formation (after Argnani and Ricchi Lucchi 2001; isopachs in the Po plain subsurface from Dondi et al. 1992) and location of the sampling sites. Marnoso Arenacea sediment sources were located mainly in the Alps but also in the Apennines, e.g., the foreland carbonate ramps of central Italy. **B)** Schematic stratigraphical log of the Marnoso Arenacea Formation (modified after Mutti et al. 2002). Solid circles indicate sampling sites (see Table 1 for geographical location): COR (Corniolo), CAB (Cabelli), GIU (Giumella), PRE (Premilcuore), BR (Bagno di Romagna).

magnetic susceptibility (AMS). The AMS, which is a measure of the crystallographic orientation of phyllosilicates and of the shape orientation of ferrimagnetic grains, has been applied to the resolution of a wide variety of problems ranging from determination of flow direction in sedimentary or igneous rocks to strain determination in deformed rocks (Parés et al. 1999 and references therein). In non-deformed sedimentary rocks, the AMS usually reflects depositional processes and geometries; still-water deposition produces a magnetic fabric with minimum susceptibility axes clustered around the pole to the depositional plane within which maximum and intermediate susceptibility axes are uniformly dispersed, defining a planar, near horizontal, gravity-induced settling fabric, whereas the magnetic fabric of sediments deposited from flowing water is typified by a current-oriented magnetic foliation that can be either horizontal or tilted (imbricated) (e.g., Ellwood 1980; Lowrie and Hirt 1987; Taira 1989; Sagnotti and Meloni 1993; Parés et al. 2007). In moderately deformed rocks, the AMS is qualitatively related to the orientation of the strain ellipsoid; the minimum susceptibility axes are normal to the cleavage and, thus, the magnetic foliation mimics the flattening plane (Parés et al. 1999; see also Sagnotti and Speranza 1993; Borradaile and Henry 1997; Cifelli et al. 2004a; Cifelli et al. 2004b; Cifelli et al. 2005; Cifelli et al. 2009).

Geological Setting

The Marnoso Arenacea Formation (hereafter MA) crops out extensively over an area of $\sim 7.2 \times 10^3$ km^2 in the northern Apennines (Fig. 1A), and is partly buried under tectonic or sedimentary units both to the west and to the northeast of its present outcrop area (Fig. 1A). The MA is a wedge-shaped, non-channelized, and mainly siliciclastic turbidite system (Ricci Lucchi 1969, 1975, 1978, 1979, 1981; Mutti and Ricci Lucchi 1972; Ricci Lucchi and Valmori 1980; Mutti et al. 2002; Amy and Talling 2006; Muzzi Magalhaes and Tinterri 2010) that represents the final stages of filling of an early to late Miocene migrating Apennine foredeep complex, accumulated between the Langhian and the Tortonian (Fig. 1B; Ricci Lucchi and Valmori 1980).

Palinspastic restorations indicate an original width of the MA basin of about 90–140 km and a sediment thickness of up to 3 km (Ricci Lucchi 1975, 1981, 1986; Boccaletti et al. 1990; Costa et al. 1998; Vai 2001). The 1 km isopach (Dondi et al. 1982; Argnani and Ricci Lucchi 2001) defines an elongated basin running at least 400 km along the Apennine front (Fig. 1A) and arranged in two main depocenters separated by the Verghereto High (Fig. 1A) (Ricci Lucchi and Valmori 1980; Amy and Talling 2006). To the southeast, the thickness of the MA decreases rapidly (Fig. 1A), suggesting the presence of an additional structural high in the Gubbio area (Argnani and Ricci Lucchi 2001).

Paleogeographic reconstructions (Mutti and Ricci Lucchi 1972; Mutti et al. 2002) coupled with petrographic (Gandolfi et al. 1983) and paleocurrent (Amy and Talling 2006; Muzzi Magalhaes and Tinterri 2010) analyses revealed that the elongated MA basin was fed mainly by Alpine (crystalline) sediments through multiple entry points located to the north and west, and flowing axially from the northwest to the southeast (in present-day coordinates) as revealed by paleocurrent directions measured at the bases of turbidite beds (Fig. 1A). In addition, minor volumes of carbonate and hybrid turbidites derived from shallow-water carbonate platforms located along the southern and southeastern margins of the basin, e.g., in the Gubbio area, are also present (Gandolfi et al. 1983; Talling et al. 2007). These carbonate and hybrid turbidites flowed from the southeast to the northwest (in present-day coordinates), i.e., in

FIG. 2.—Examples of Marnoso Arenacea Formation outcrops at Castel del Rio showing fine-to medium-grained turbidites (*), the associated Bouma's T_e divisions (**), and the WM beds (***); the WM beds can be distinguished from Bouma's T_e divisions by their lighter color as a result of greater carbonate content and lesser total-organic-carbon content.

the direction opposite to that of the aforementioned siliciclastic turbidites, and comprise key marker beds such as the Contessa and Colombine megaturbidites that allow high-resolution stratigraphic correlations at the basin scale. Furthermore, slumps and turbidite flows have been reported coming also from active thrust fronts located to the west of the basin (Ricci Lucchi 1975). The ability of flows to traverse the basin in opposite directions implies low sea-floor gradients (Ricci Lucchi and Valmori 1980; Amy and Talling 2006). Paleobathymetric estimates from $\delta^{18}O$ data on benthic foraminifera indicate a wide range of upper to mid-bathyal water depths (Aharon and Sen Gupta 1994).

The White Marlstones Beds (WM beds)

The WM beds consist of $<$ 20-cm-thick (rarely $>$ 50-cm-thick) intervals of cohesive clay and silt with grain size generally ranging from 0.5 to 50 μm (Talling et al. 2007). They overlie in rapid vertical transition dark blue-gray Bouma's T_e intervals of the associated MA siliciclastic turbidites, from which they can be distinguished by their texture, lighter color (Fig. 2), greater carbonate content (from 25% to 45%), and lower total organic content (TOC $\approx$ 1% in WM beds compared to TOC $\approx$ 2% in Bouma's T_e divisions). The carbonate content of the WM beds is represented chiefly by planktonic foraminifera and coccoliths, and rare benthic foraminifera (Fig. 3, white arrows); mica (Fig. 3, black arrows), illite, and dolomite have also been observed. This overall composition is reminiscent of the composition of mudstone intervals of carbonate and hybrid turbidites derived from shallow-water carbonate platforms located along the southern and southeastern margins of the basin (e.g., Gubbio area; Fig. 1A) (Gandolfi et al. 1983; Talling et al. 2007).

Our observations indicate that the WM beds are characterized by a massive, ungraded, speckled, and generally featureless aspect with rare parallel laminations, from 0.2 mm to 1.0 mm thick, picked out by concentrations of silt with modal size of 10 μm or by the occurrence of irregular shelly concentrations. Laminae can also be arranged in centimeter- to decimeter-thick stacks of alternating fine silt and clayey silt. The vertical distribution of laminae, as well as of bed thickness, composition, and color, appears to be random throughout the WM beds. Primary sedimentary structures have been partly destroyed by moderate but relatively continuous bioturbation, indicating sedimentation rates sufficiently low to prevent major disturbance of the benthic infauna (McBridge and Picard 1991; Monaco and Checconi 2008; Monaco 2008). The analysis of numerous published stratigraphic sections (Ricci Lucchi and Valmori 1980; Talling 2001; Mutti et al. 2002) and basin-scale high-resolution correlations (Amy and Talling 2006; Talling et al. 2007; Muzzi Magalhaes and Tinterri 2010; Talling et al. 2012a; Talling et al. 2012b) indicate no relationship between thickness and frequency distribution of the WM beds relative to the associated MA turbidites, which seems to indicate that WM beds and MA turbidites are genetically unrelated (see also discussion below). The general downcurrent (i.e., southward) thinning of turbidites, including Bouma's T_e divisions, is accompanied by an overall thickening of the WM beds. The maximum cumulative thickness of the WM beds occurs on the down-flow side of the Verghereto High (Talling et al. 2007).

The average rate of sediment accumulation inferred from biostratigraphically dated sections from the literature (Ricci Lucchi and Valmori 1980; Talling 2001; Mutti et al. 2002; Amy and Talling 2006; Talling at al. 2007; Muzzi Magalhaes and Tinterri 2010) is of about 3 cm/kyr. These values are comparable to sedimentation rates of similar deposits worldwide ($<$ 2 cm/kyr for compacted pelagic sediments from the Solomon Islands (Colwell and Exon 1988), from 5 cm/kyr to 15 cm/kyr for compacted hemipelagic sediments from the Oman margin, and 3–10 cm/kyr for contouritic sheeted drifts from Oman margin (Stow and Tabrez 1998)), and are lower than rates of 20 cm/kyr for modern and uncompacted hemipelagic muds (East Japan Sea; Park et al. 2006).

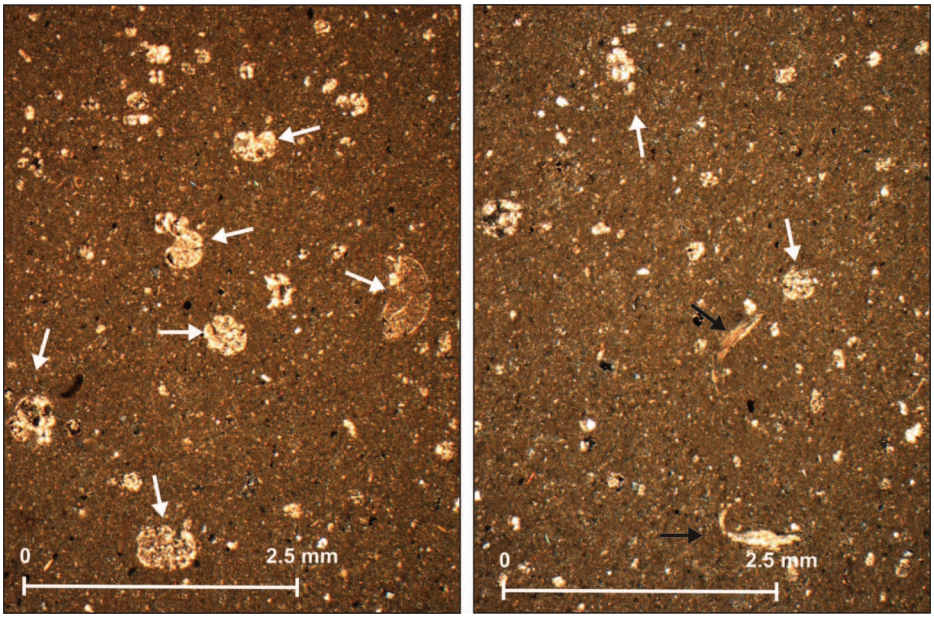

FIG. 3.—Thin sections of representative WM beds, characterized by high carbonate content (~ 45%; chiefly pelagic foraminifers) and grain size between mud and silt. White arrows indicate pelagic foraminifers (*Globigerinoides*), and black arrows indicate muscovite minerals of the mica group, probably representing the main source of the (para)magnetic-susceptibility signal.

The Anisotropy of Magnetic Susceptibility

The magnetic susceptibility is a second-rank symmetric tensor, k_{ij}, which relates the magnetization J_i induced in a sample by a field H_i, according to the formula $J_i = k_{ij} H_j$. The anisotropy of magnetic susceptibility (AMS) can be specified by six quantities, three relating to the magnitude of the principal susceptibility axes (k_{max}, k_{int}, k_{min}) and three relating to their directions, which are mutually orthogonal.

In sedimentologic analyses, the AMS is considered to be a proxy for the preferred alignment of natural magnetic particles attained in the final stages of sediment transport, with the maximum-susceptibility axis, k_{max}, and the minimum-susceptibility axis, k_{min}, representing the preferred orientation of the longest and shortest magnetic grain axes, respectively (e.g., Hamilton and Rees 1970; Taira and Scholle 1979). This method is based on the fact that a current is able to orient paramagnetic grains (e.g., phyllosilicates, olivines, pyroxenes, amphiboles), diamagnetic grains (e.g., quartz, calcite, feldspars), and ferromagnetic (*sensu lato*) grains (e.g., magnetite, hematite), and that the resulting AMS ellipsoid reflects the orientation imparted by the current to such grains (Parés et al. 2007).

AMS in sediments may develop during and after deposition. During settling of grains, e.g., phyllosilicates, on the sea floor, their short shape axes usually fall perpendicular to the bedding plane. As a result, an oblate fabric develops (well-developed foliation). The AMS fabric mimics this sedimentary fabric because in phyllosilicates, the short shape axis corresponds to the crystallographic *c* axis as well as to the minimum-susceptibility direction, and, therefore, a magnetic foliation (defined by the plane containing k_{max} and k_{int} axes) develops parallel to the depositional surface.

When currents are present, hydraulic forces control the alignment of the grains (current-induced fabric; Shor et al. 1984). Elongated particles suspended in a moderate-velocity flow typically travel in upright (vertical) position until they touch the bottom and rotate parallel to the flow direction. Flow-aligned fabrics arise when grains are subjected to a combination of minimal drag and negative lift forces that tend to push particles down onto the seabed (Pettijohn 1975; Collinson and Thompson 1982; Allen 1984). Such flow-aligned orientations can sometime evolve into flow-transverse orientations when strong currents are capable of lifting and displacing grains after initial deposition (Schwarzacher 1963; Johansson 1964; Hendry 1976). In contrast to suspended particles, bedload particles typically roll on the seabed with the long shape axis perpendicular to the main flow direction (Baas et al. 2007), producing what is often called a "rolling" fabric (Harms et al. 1982).

The AMS fabric reflects the orientation of elongated paramagnetic as well as large ferromagnetic grains either parallel or perpendicular to the current direction, because in such elongated grains the maximum-susceptibility axis commonly lies broadly along (or at a small angle to) the particle length. Consequently, a magnetic lineation can develop as revealed by a clustering of the k_{max} axes either parallel or perpendicular to the current direction, depending on the hydrodynamic boundary conditions.

After deposition, the fabric may be affected by compaction and tectonic deformation. As pointed out by Parés et al. (1999), there is general agreement in studies dealing with AMS development in deformed rocks (e.g., Borradaile and Tarling 1981, 1984; Kissel et al. 1986; Averbuch et al. 1992; Parés and Dinarés-Turell 1993; Sagnotti and Speranza 1993; Aubourg et al. 1995; Mattei et al. 1995) that the first effect of layer-parallel shortening is to group the k_{max} axes perpendicular to the shortening direction (whereas the k_{min} axes tend to remain perpendicular to the bedding plane); with further shortening, the k_{min} axes progressively rotate into the tectonic shortening direction, and the magnetic foliation becomes parallel to the flattening plane and mesoscopic cleavage (examples of this sedimentary to tectonic fabric progression are provided by Housen et al. (1995), Averbuch et al. (1992), and Parés et al. (1999)). Hence, in order to discriminate between sedimentary and tectonic fabrics, the relationships between the AMS and the geometry of sedimentary and tectonic features must be studied in detail.

MATERIALS AND METHODS

AMS analyses were carried out on 93 cylindrical (10.3 cm^3) oriented samples collected in nine distinct WM beds from five selected stratigraphic sections (Fig. 1; Table 1; Talling et al. 2012a; Talling et al. 2012b) with a water-cooled drill, and oriented with a magnetic compass. All sampled WM beds overlie Bouma's T_e intervals of MA siliciclastic turbidites flowing axially from the northwest to the southeast (in present-day coordinates). The susceptibility of each specimen was measured in 15 directions with a KLY-3 Kappabridge adopting the standard measurement scheme of Jelinek (1978). A susceptibility tensor was then fit to the data by means of least-squares analysis, and errors were calculated using multivariate statistics (Jelinek 1978) with the software Anisoft 4.2. Each susceptibility tensor was subsequently rotated into tilt-corrected coordinates using

TABLE 1.—*Geographic location of sampling sites.*

Location	Site Abbreviations	Lattitude	Longitude
Bagno di Romagna	BR	43°49′27.87″ N	11°57′30.06″ E
Cabelli	CAB	43°55′50.87″ N	11°51′7.40″ E
Castelpriore	CP	43°49′29.47″ N	12°7′21.00″ E
Corniolo	COR	43°54′30.54″ N	11°47′41.80″ E
Giumella	GIU	43°58′7.75″ N	11°45′44.36″ E
Premilcuore	PRE	43°58′45.52″ N	11°46′53.31″ E

site-mean bedding attitudes and plotted on stereographic projections. We also obtained for each site the *magnetic lineation* $L = k_{max}/k_{int}$ (Balsley and Buddington 1960), the *magnetic foliation* $F = k_{int}/k_{min}$ (Stacey et al. 1960), the *shape parameter* $T = (\log_e F - \log_e L) / (\log_e F - \log_e L)$ (Jelinek 1981), the *anisotropy degree* $P = k_{max}/k_{min}$, and the *corrected anisotropy degree* $P' = P^{\alpha}$ where $\alpha = \sqrt{(1 + T^2/3)}$ (Jelinek 1981). Oblate (foliated) and prolate (lineated) fabrics were plotted on Flinn-type diagrams (Hrouda 1982; Tarling and Hrouda 1993) and on shape-anisotropy degree ($T - P'$) diagrams (Jelinek 1981).

To determine the ferromagnetic mineralogy of the sediments potentially contributing to the AMS, representative samples were subjected to stepwise acquisition of an isothermal remanent magnetization (IRM) up to 2.5 T with an ASC Pulse Magnetizer. Samples were then subjected to thermal demagnetization of a three-component IRM imparted in 2.5 T, 1.0 T, and 0.1 T orthogonal fields (Lowrie 1990). A second suite of fresh samples was subjected to thermal demagnetization of the natural remanent magnetization (NRM) in order to isolate magnetic-component directions potentially present in the WM beds. IRM and NRM measurements were made on a 2G DC SQUID cryogenic magnetometer placed in a magnetically shielded room in the Alpine Laboratory of Paleomagnetism of Peveragno, Italy.

RESULTS

Equal-area stereographic projections of the k_{max}, k_{int},and k_{min} susceptibility axes of the studied samples are plotted in Figure 4A before correction for bedding tilt, and in Figure 4B after correction for bedding tilt; the susceptibility values plus additional parameters discussed in the text, averaged at the site level, are reported in Table 2. A well-preserved anisotropic fabric with clustered k_{max}, k_{int}, and k_{min} axes is evident in all sites in geographic (*in situ*) coordinates (Fig. 4A); the k_{max} axes tend to be subparallel to the flow directions measured by sedimentological markers (e.g., flute casts) at the base of the nearest turbidite bed (Fig. 4A, blue arrows), as well as to the strike of bedding planes (Fig. 4A; we will return to this coincidence between k_{max} and bedding strike further below). Upon correction for bedding tilt, the k_{min} axes become substantially vertical, i.e., perpendicular to the bedding planes, whereas the k_{max} axes are consistently horizontal, i.e., parallel to the bedding planes (and subparallel to the flow directions) (Fig. 4B). This is evident also from the statistical distribution of the susceptibility axes of all samples ($n = 93$) upon rotation from geographic (*in situ*) coordinates (Fig. 5A) to tilt-corrected coordinates

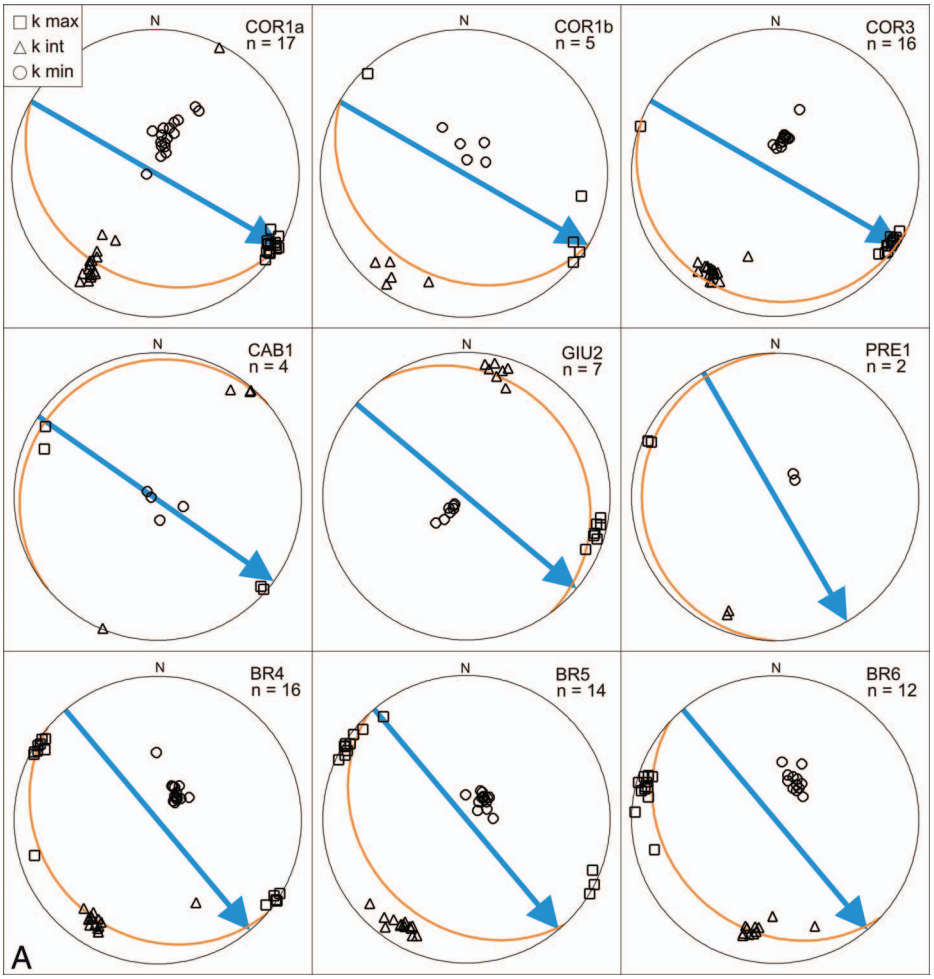

(Fig. 5B): Fisher's (1953) statistics indicate that the overall mean k_{min} direction in geographic coordinates (Declination = 23.5° E; Inclination = 73.8°; precision parameter k = 38; cone of 95% confidence around the mean α_{95} = 2.4°; n = 93) becomes subvertical and better grouped after correction for bedding tilt (Dec. = 278.7° E; Inc. = 85.7°; k = 52; α_{95} = 2.0°; n = 93), with the precision parameter k increasing by ~ 1.4 upon full (100%) tilt correction (Fig. 5A, B). The tilt-corrected k_{max} axes are oriented northwest–southeast (mean of 298° E–118° E) in present-day coordinates, i.e., without correction for Apennine thrust-sheet rotation (Fig. 5C, black distribution). The anisotropy degree P and the corrected anisotropy degree P_j are relatively low, saved for COR3 samples, characterized by $P_j > 1.06$ (Fig. 5D; Table 2); the shape parameter T plotted versus P_j indicates slightly oblate or slightly prolate fabrics (Fig. 5D), as do the Flinn-type plot (Fig. 5E). Notably, purely foliated fabrics with k_{max} and k_{int} axes scattered in the depositional plane (Parés et al. 2007) have not been observed.

The observed magnetic fabric could be due to the presence of paramagnetic and/or ferromagnetic (s.l.) grains. Slightly elongated paramagnetic phyllosilicates (muscovite; Fig. 3, black arrows) have frequently been observed by image analysis in thin sections in association with abundant diamagnetic carbonates. The analyses of the IRM acquisition and thermal demagnetization of a three-component IRM reveal the presence of a low-coercivity ferromagnetic phase with maximum unblocking temperatures of ~ 570 °C interpreted as magnetite (Fig. 6). Hence, we conclude that paramagnetic muscovite and possibly also magnetite grains control the observed AMS fabric. Finally, the thermal demagnetization of the NRM reveals that this magnetite carries no stable magnetic-component directions saved for an initial (low-temperature) viscous overprint broadly oriented along the present-day field direction in *in situ* coordinates. Hence, these NRM data could not provide a means to correct the observed AMS fabric for Apennine thrust-sheet rotation, which will be performed using data from the literature (Speranza et al. 1997; Muttoni et al. 1998, 2000), after a discussion on the origin (sedimentary or tectonic) of the magnetic fabric.

Interpretation: Sedimentary Versus Tectonic Origin of the AMS Fabric

The k_{max} axes of the WM beds are virtually parallel to the average flow direction measured by flute casts at the base of turbidite beds. They are also parallel to the basin axis (corresponding to the elongation of the Miocene Apennine foredeep) and to the lateral confining slopes of the MA basin. This substantial parallelism (coupled with the vertical distribution of the k_{min} axes in tilt-corrected coordinates) tends to suggest a sedimentological, current-induced origin for the observed magnetic fabric. However, Apennine compression is oriented northeast–southwest in the investigated area, which exhibits a degree of deformation of up to about 50% shortening (Ricci Lucchi 1975; Ricci Lucchi 1981; Ricci Lucchi 1986; Boccaletti et al. 1990; Costa et al. 1998; Vai 2001). Therefore, the associated compressional structures (thrust planes, fold axes) are regionally oriented NW–SE and therefore result broadly parallel to the observed k_{max} axes. This introduces a potential ambiguity on the origin of the magnetic

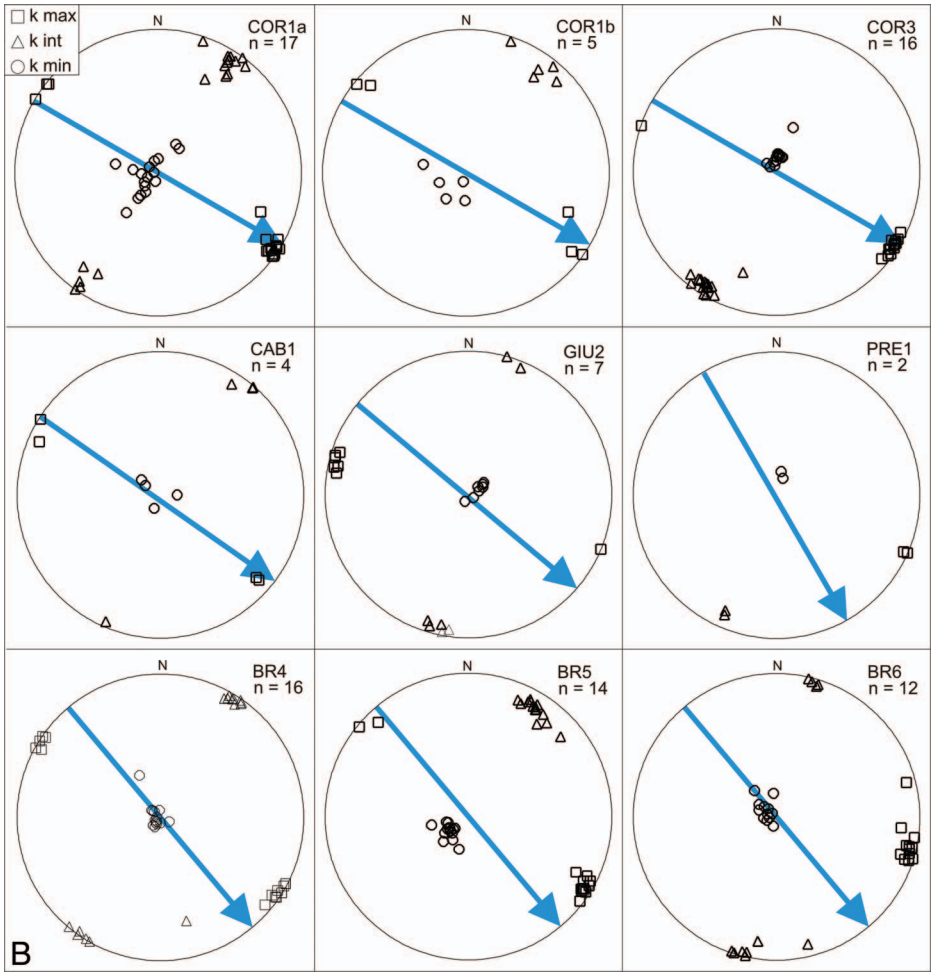

FIG. 4.—Representative stereographic projections of the principal susceptibility axes of the magnetic anisotropy, in **A)** *in situ* and **B)** tilt-corrected coordinates (see Table 2 for data). Each plot corresponds to a given sampling site (for sites location, see Fig. 1A). A depositional anisotropic fabric with clustered k_{max} (squares), k_{int} (triangles), and k_{min} (circles) susceptibility axes is evident in all WM beds sites and defines a magnetic lineation (cluster of k_{max} axes) oriented approximately northwest–southeast (without correction for Apennine thrust-sheet rotation), whereas the minimum susceptibility axes are oriented vertical, i.e., perpendicular to the bedding plane. COR1a, COR1b, COR3, CAB1, GIU2, PRE1, BR4, BR5, BR6 = sampling sites (see Fig. 1 for acronyms and location); n = number of samples per site; blue arrow = paleocurrent direction from flute marks; orange great circle = strike of the bedding plane.

TABLE 2.—*AMS parameters of the WM beds.*

	n	K_{mean} ± σ [*10E − 6SI]	K_{max} ± σ [*10E − 6SI]	K_{int} ± σ [*10E − 6SI]	K_{min} ± σ [*10E − 6SI]	L ± σ	F ± σ	P ± σ	P_j ± σ	T ± σ
COR1a	17	146.66 ± 39.90	149.67 ± 40.72	145.96 ± 39.69	144.37 ± 39.28	1.0253 ± 0.0023	1.0113 ± 0.0029	1.0370 ± 0.0029	1.0379 ± 0.0028	−0.3837 ± 0.1324
COR1b	5	161.74 ± 2.05	165.41 ± 2.14	161.47 ± 2.06	158.35 ± 1.96	1.0244 ± 1.0010	1.0197 ± 0.0015	1.0446 ± 0.0020	1.0447 ± 0.0020	−0.1058 ± 0.0373
COR13	16	189.24 ± 8.45	195.70 ± 8.55	191.63 ± 8.37	180.39 ± 8.52	1.0213 ± 0.0019	1.0625 ± 0.0102	1.0851 ± 0.0097	1.0886 ± 0.0110	0.4772 ± 0.0833
CAB1	4	163.55 ± 11.85	166.89 ± 12.14	164.03 ± 11.89	159.73 ± 11.55	1.0174 ± 0.0005	1.0269 ± 0.0030	1.0448 ± 0.0031	1.0452 ± 0.0033	0.2096 ± 0.0544
GIU2	7	153.66 ± 6.89	157.02 ± 6.99	154.28 ± 6.99	149.66 ± 6.71	1.0178 ± 0.0012	1.0309 ± 0.0043	1.0492 ± 0.0041	1.0498 ± 0.0045	0.2611 ± 0.0782
PRE1	2	156.60 ± 4.09	160.17 ± 4.04	157.79 ± 4.40	151.84 ± 3.84	1.0151 ± 0.0027	1.0392 ± 0.0027	1.0549 ± 0.0001	1.0567 ± 0.0007	0.4395 ± 0.0983
BR4	16	141.75 ± 4.78	144.31 ± 4.65	142.01 ± 4.59	138.93 ± 4.81	1.0161 ± 0.0033	1.0223 ± 0.0046	1.0387 ± 0.0018	1.0391 ± 0.0018	0.1540 ± 0.2084
BR5	14	138.89 ± 5.06	141.65 ± 5.30	139.65 ± 5.18	135.37 ± 4.71	1.0143 ± 0.0007	1.0316 ± 0.0040	1.0463 ± 0.0042	1.0474 ± 0.0047	0.3688 ± 0.0549
BR6	12	173.65 ± 23.64	177.11 ± 24.96	175.17 ± 24.39	168.68 ± 21.61	1.0109 ± 0.0020	1.0374 ± 0.0118	1.0487 ± 0.0136	1.0511 ± 0.0148	0.5339 ± 0.0631

n = number of samples per site; $K_{mean} = (k_{max} + k_{int} + k_{min})/3$ (mean susceptibility); k_{max} = maximum susceptibility; k_{int} = intermediate susceptibility; k_{min} = minimum susceptibility; $L = k_{max}/k_{int}$ (magnetic lineation); $F = k_{int}/k_{min}$ (magnetic foliation); σ = standard deviation from the mean; $P = k_{max}/k_{min}$ (anisotropy degree); $P_j = \exp\sqrt{2}\{(\eta 1 - \eta)2 + (\eta 2 - \eta)2 + (\eta 3 - \eta)2\}$ (corrected anisotropy degree − Jelinek 1981); $T = 2(\eta 2 - \eta 3)/(\eta 1 - \eta 3) - 1$ (shape parameter − Jelinek 1981) ; $\eta 1 = \ln k_{max}$; $\eta 2 = \ln k_{int}$; $\eta 3 = \ln k_{min}$; $\eta = (\eta 1 + \eta 2 + \eta 3)/3$.

fabric, i.e., sedimentary versus tectonic. This ambiguity is evident for sites COR1a, COR1b, COR3, and BR4, which are characterized by k_{max} axes oriented subparallel to the paleoflow direction calculated from the nearest flute casts as well as to the strike of the tectonically tilted strata sampled for AMS (Fig. 4A). Sites CAB1 and PRE1—albeit characterized by sparse data—show k_{max} axes that are again oriented parallel to the paleoflow directions, but in contrast to the previous cases, both quantities lie at a high angle with the bedding strikes, a geometry regarded as less compatible with a tectonic control on the AMS. In any case, following studies of sedimentary to tectonic fabric progression in deformed rocks (e.g., Borradaile and Tarling 1981, 1984; Kissel et al. 1986; Averbuch et al. 1992; Parés and Dinarés-Turell 1993; Sagnotti and Speranza 1993; Aubourg et al. 1995; Mattei et al. 1995; Parés et al. 1999; see also Cifelli et al. 2004a; Cifelli et al. 2004b; Cifelli et al. 2005; Cifelli et al. 2009), at the stage of deformation versus shortening observed in the investigated area ("weak cleavage stage"; Parés et al. 1999), the k_{min} should be distributed along a girdle parallel to the tectonic shortening direction, and the magnetic ellipsoid should be prolate. Instead, our data (Figs. 4, 5) do not show this pattern whereby the k_{min} axes are consistently vertical in tilt-corrected coordinates, i.e., perpendicular to the bedding planes, whereas the k_{max} axes are consistently horizontal, i.e., parallel to the bedding planes, and oriented northwest–southeast.

As a test to resolve the ambiguity, we sampled for AMS nearby turbidite intervals that are markedly different from the WM beds from a depositional viewpoint, but as similar as possible to the WM beds from a granulometric (~ rheologic) viewpoint. We selected very fine-grained sandstones with convolute lamination due to water escape processes, and found that they are characterized by highly scattered susceptibility-axes orientations (Fig. 7A, B). These data are taken as evidence of a sedimentological control on the AMS whereby water-escape processes are expected to disrupt originally laminated or planar fabrics, thereby inducing the observed scattering. Another example is given by debrites, which result from *en masse* deposition of cohesive flows that is expected to generate scattered AMS fabrics, as indeed observed in our sampled debrite intervals (Fig. 7C).

Based on these data, we favor the hypothesis of a substantial sedimentary, current-induced origin of the magnetic fabric of the WM beds, albeit the conundrum regarding a potential contribution from deformation is admittedly not completely resolved, e.g., at site BR5 with nonvertical k_{min} axes after bedding tilt correction (Fig. 4B). Currents should have flowed along the longitudinal basin axis that we corrected for Apennine thrust-sheet rotations by applying to the mean k_{max} direction a clockwise rotation of 29° (± 8°) as suggested by Speranza et al. (1997) and Muttoni et al. (1998, 2000) for Oligo-Miocene sediments from the same general area of this study, obtaining a corrected NNW–SSE direction (330°E) that approximates the Miocene paleoflow direction along the axis of the Marnoso Arenacea longitudinal basin (Fig. 5C; gray distribution).

DISCUSSION AND CONCLUSIONS

A largely current-induced AMS fabric implies that the WM beds cannot be explained considering simply hemipelagic settling of deep-sea mud because hemipelagic deposition of, e.g., phyllosilicates gives rise to purely foliated fabrics with no preferred k_{max} and k_{int} orientation (e.g., Ellwood 1980; Lowrie and Hirt 1987; Taira 1989; Sagnotti and Meloni 1993; Parés et al. 2007). Excluding purely hemipelagic settling, the WM beds could arise from two alternative depositional mechanisms: turbidity currents or bottom currents, as described hereafter.

Turbidity Currents

The WM beds could have been derived from the settling of suspension clouds produced from fading turbidity currents (hemiturbidites *sensu*

Stow and Wetzel 1990). During a turbidity-current event, thick and relatively diluted turbulent flows could have detached from the basal and denser part of the flow at gentle bends along the axial flow path (as described for the Navy Fan of the California borderland; Normark and Piper 1972). These diluted flows may have moved high along basin-bordering slopes where they eroded and incorporated carbonate-rich sediments, to be eventually deflected and forced to rejoin the axial zone farther downcurrent after deposition of the denser axial flow (Mutti et al. 2002; Muzzi Magalhaes and Tinterri 2010). In this interpretation, sketched in Figure 8A, a single large-volume turbidity event can generate a stack of several delayed, ponded WM beds above its main axial deposit of medium-grained sand.

A turbidite origin implies that the flows, after dropping the heavier terrigenous load, began depositing lighter particles, e.g., abundant carbonate shells (e.g., coccoliths and other hydraulically equivalent clay-size carbonate particles) and phyllosilicates. This indicates that the WM beds may have resulted from hydraulic sorting of the finer and lighter particles toward the upper part of the flow, and may constitute the distal end members of turbidite facies tracts (end of Bouma's T_e division). Calcite is denser than clay minerals, but clay minerals flocculate more effectively than carbonates (Piper 1978; Stow et al. 1984), forming from 10 μm to 50 μm flocs that are much larger than the typical micritic carbonate particles (from 1 μm to 3 μm) (Piper 1978; Stow et al. 1984); thus, when large amounts of fine carbonates are present, their concentration tends to increase near the top of turbidity currents because these particles have a lower tendency to form large flocs.

The settling of a suspension cloud at the end of a turbidity flow may have been facilitated by reductions in bathymetric gradient and by flow ponding toward the southern part of the basin, or by the presence of intrabasinal topographic highs and/or slope changes that triggered flow deceleration and mud-erosion processes (Muzzi Magalhaes and Tinterri 2010). Similar depositional mechanisms have been proposed by Remacha et al. (2005) for basin-plain calcilutites in the Hecho Basin (south-central Pyrenees, Spain), by Carruba et al. (2004, 2007) and Felletti et al. (2009) in the Cellino Periadriatic foredeep (Central Italy), and by Felletti (2004) and Felletti and Bersezio (2010a, 2010b) for ponded turbidite systems in the Tertiary Piedmont Basin (NW Italy).

Bottom Currents

The WM beds could represent muddy contourites deposited from semipermanent bottom currents flowing parallel to the basin axis (Fig. 8B), similarly to what observed along slope settings elsewhere (Stow and Lovell 1979; Stow 1982; Gonthier et al. 1984; Howe 1995, 1996; Stow and Tabrez 1998). Light particles such as carbonate shells and phyllosilicates could have been incorporated into bottom currents by particle lofting and resuspension. The AMS analysis indicates that these currents were relatively constant in direction, whereas sedimentological indicators (sorting, homogenization by bioturbation, and absence of erosional surfaces) point to weak current velocities, in the range of 0.05 m s^{-1} and 0.15 m s^{-1} as derived from the "bedform velocity matrix" proposed by Stow et al. (2009). The WM beds commonly contain bimodal admixtures of cohesive silt and clay characterized by poor sorting. These characteristics are all commensurate with transport of a mixed-composition load followed by deposition directly from suspension. The occurrence of irregular shelly concentrations and of alternating fine silt and mud laminae, some of which show internal grading, possibly indicates small fluctuations in current strength during deposition of WM beds.

Because the WM beds show a composition similar to the turbidites derived from the carbonate platforms located along the southeastern margin of the basin (Gandolfi et al. 1983; Talling et al. 2007), we infer that the bottom currents also originated in the southeast and flowed northwestward (Fig. 8B) parallel to the basin axis and in the direction opposite to that of the MA siliciclastic turbidites (Fig. 8A). The imbricated magnetic fabric observed in site COR 1b (Fig. 4A, B), with the k_{max} axis plunging to the southeast, supports this interpretation.

We favor the hypothesis that the WM beds represent muddy contourites, based on the following arguments:

(i) The vertical distribution of thickness and frequency of the WM beds appears to be random compared to the bedding thickness distribution of the associated turbidites (Talling 2001; Amy and Talling 2006; Talling et al. 2007). In particular, thick WM beds frequently overlie very thin and fine-grained MA turbidites, whereas thick turbidites may underlie thin WM beds. This evidence suggests that the MA turbidites and the WM beds are not related statistically (and presumably also genetically); consequently, the WM beds can hardly represent the distal end members of turbiditic facies tracts.

(ii) The vertical distribution of laminae, sedimentary structures, composition, and color appear to be random throughout the WM beds. Instead, if the WM beds were derived from the settling of suspension clouds produced from fading turbidity currents, we would expect systematic vertical variations of the aforementioned features as described by Piper (1978), Mulder et al. (2008), and Mulder et al. (2009).

(iii) Several sedimentological features of the WM beds seem to be more consistent with standard contourite models (Piper 1978; Stow and Lovell 1979; Stow 1982; Gonthier et al. 1984; Howe 1995, 1996; Stow and Tabrez 1998; Mulder et al. 2008; Mulder et al. 2009; Stow and Faugères 2008) than with turbidite models (Piper 1978; Stow and Faugères 2008; Mulder et al. 2008; Mulder et al. 2009). These features include the occurrence of (1) relatively continuous, moderate bioturbation, indicating sedimentation rates sufficiently low to prevent major disturbances to the infauna, (2) parallel laminations, and (3) irregular shelly concentrations.

Our interpretation of the WM beds as muddy contourites does not exclude in any case the effects of reworking by contour currents of fine-grained material originally supplied by turbidity currents, as demonstrated in similar depositional systems elsewhere (Rebesco et al. 1996; Rebesco et al. 1997; Pudsey 2000; Escutia et al. 2000; Knutz et al. 2002).

ACKNOWLEDGMENTS

Francesca Cifelli and an anonymous reviewer are thanked for helpful comments. G. Malgesini is warmly acknowledged for his help during field work. Financial support was provided by FIRB (Fondo per gli Investimenti della Ricerca di Base) 2006–2009 funds to F. Felletti, and International Association of Sedimentologists grant to E. Dall'Olio.

REFERENCES

Aharon, P., and Sen Gupta, B.K., 1994, Bathymetric reconstructions of the Miocene-age "calcari a Lucina" (Northern Apennines, Italy) from oxygen isotopes and benthic Foraminifera: Geo-Marine Letters, v. 14, p. 219–230.

Allen, J.R.L., 1984, Sedimentary Structures; their Character and Physical Basis: Amsterdam, Elsevier, Developments in Sedimentology, v. 30, p. 593–663.

Amy, L., and Talling, P.J., 2006, Anatomy of turbidites and linked debrites based on long distance (120 × 30 km) bed correlation, Marnoso Arenacea Formation, Northern Apennines, Italy: Sedimentology, v. 53, p. 161–212.

Argnani, A., and Ricci Lucchi, F., 2001, Tertiary siliciclastic turbidite systems of the Northern Apennines, *in* Vai, G.B., and Martini, P., eds., Apennines and Adjacent Mediterranean Basins: Dordrecht, Kluwer Academic Publishers, p. 327–350.

Aubourg, C., Rochette, P., and Bergmüller, F., 1995, Composite magnetic fabric in weakly deformed black shales: Physics of the Earth and Planetary Interiors, v. 87, p. 267–278.

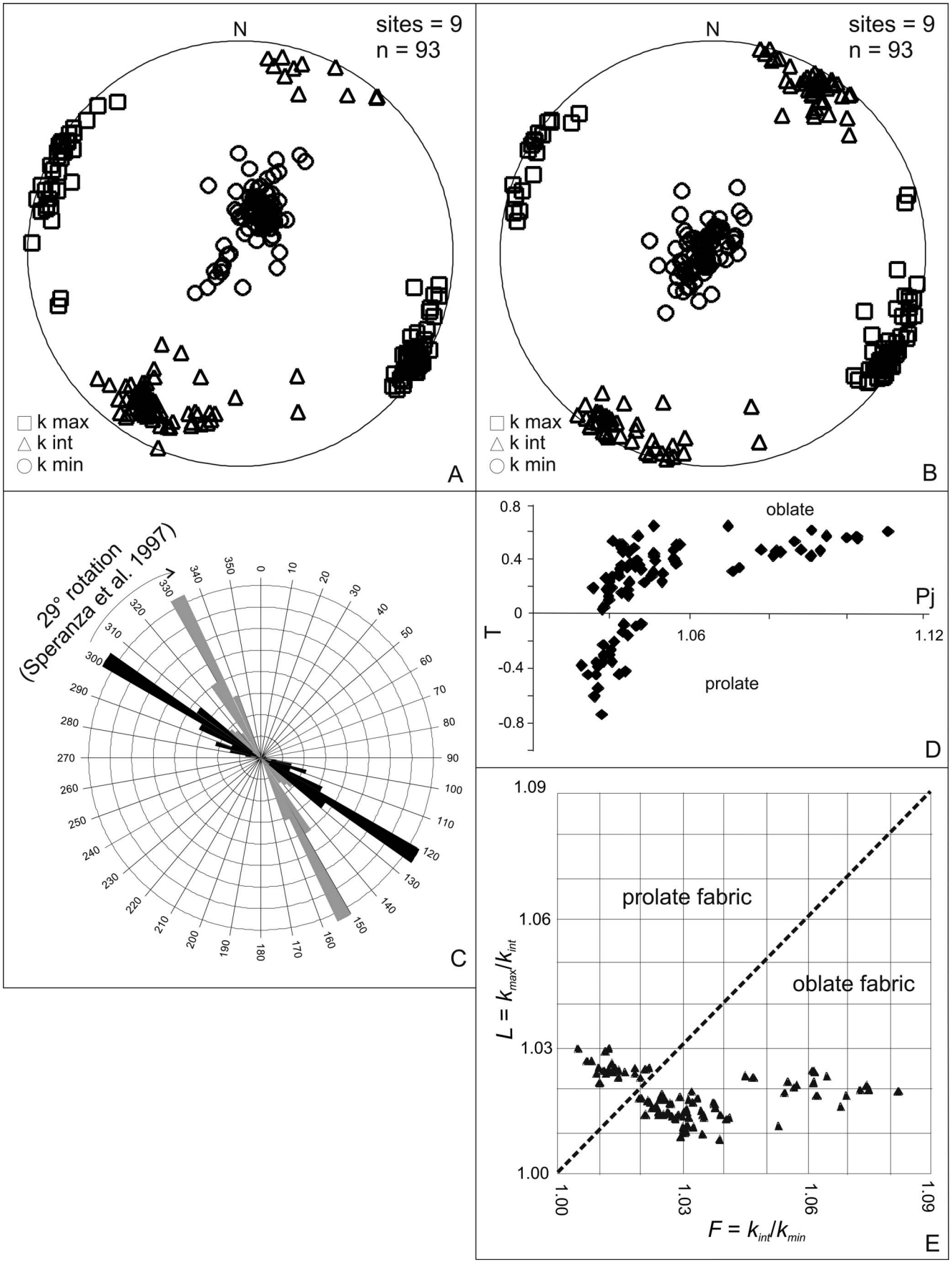
N
sites = 9
n = 93
k max
k int
k min
A
B
29° rotation
(Speranza et al. 1997)
C
oblate
prolate
Pj
T
0.8
0.4
0
-0.4
-0.8
1.06
1.12
D
prolate fabric
oblate fabric
L = k_{max}/k_{int}
F = k_{int}/k_{min}
1.09
1.06
1.03
1.00
E

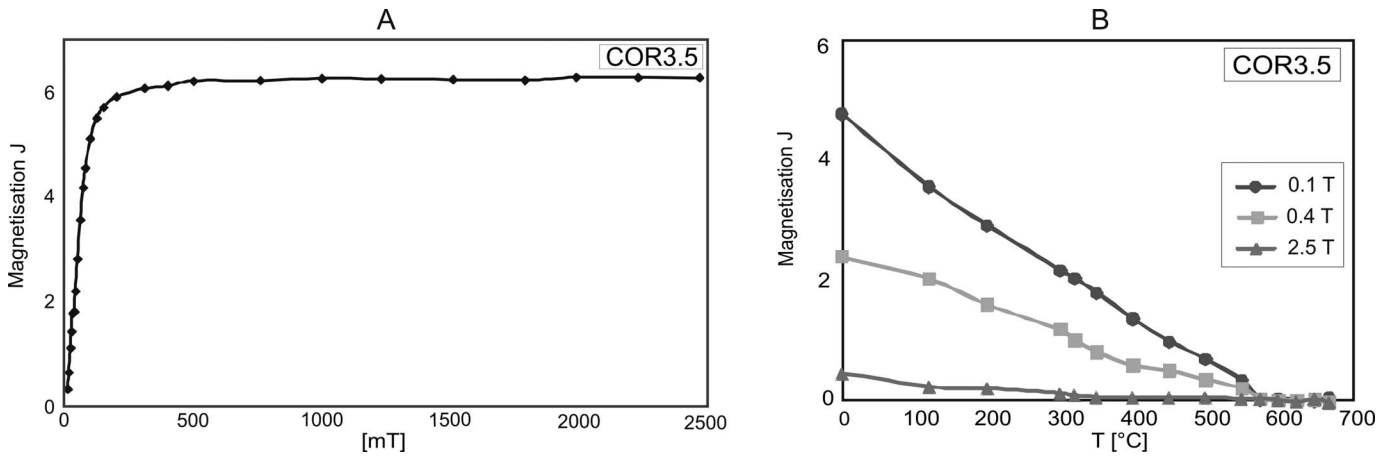

FIG. 6.—**A)** Isothermal-remanent magnetization (IRM) acquisition curve and **B)** thermal decay of a three-component IRM (right panel) for representative sample COR3.5, indicating the presence of magnetite (see text for discussion).

AVERBUCH, O., FRIZON DE LAMOTTE , D., AND KISSEL, C., 1992, Magnetic fabric as a structural indicator of the deformation path within a fold-thrust structure: a test case from the Corbieres (NE Pyrenees, France): Journal of Structural Geology, v. 14, p. 461–474.

BAAS, J.H., HAILWOOD, E.A., MCCAFFREY, W.D., KAYC, M., AND JONES, R., 2007, Directional petrological characterisation of deep-marine sandstones using grain fabric and permeability anisotropy: methodologies, theory, application and suggestions for integration: Earth-Science Reviews, v. 82, p. 101–142.

BALSLEY, J.R., AND BUDDINGTON, A.F., 1960, Magnetic susceptibility anisotropy and fabric of some Adirondack granites and orthogneisses: American Journal of Science, v. 258, p. 6–20.

BOCCALETTI, M., CALAMITA, F., DEIANA, G., GELATI, R., MASSARI, F., MORATTI, G., AND RICCI LUCCHI, F., 1990, Migrating foredeep-thrust belt system in the northern Apennines and southern Alps: Palaeogeography, Palaeoclimatology, Palaeoecology, v. 77, p. 3–14.

BORRADAILE, G.J., AND HENRY, B., 1997, Tectonic application of magnetic susceptibility and its anisotropy: Earth-Science Reviews, v. 42, p. 49–93.

BORRADAILE, G.J., AND TARLING, D., 1981, The influence of deformation mechanisms on magnetic fabrics in weakly deformed rocks: Tectonophysics, v. 77, p. 151–168.

BORRADAILE, G.J., AND TARLING, D., 1984, Strain partitioning and magnetic fabrics in particulate flow: Canadian Journal of Earth Sciences, v. 21, p. 694–697.

CARRUBA, S., CASNEDI, R., AND FELLETTI, F., 2004, From seismic to bed: surface–subsurface correlations within the turbiditic Cellino Formation (Central Italy): Petroleum Geoscience, v. 10, p. 131–140.

CARRUBA, S., CASNEDI, R., AND FELLETTI, F., 2007, Sedimentary evolution in a migrating basin: geometry and facies analysis of the sandy bodies in the Cellino Formation (Lower Pliocene Periadriatic foredeep, Central Italy): Società Geologica Italiana, Bollettino, v. 126, p. 473–485.

CIFELLI, F., ROSSETTI, F., MATTEI, M., HIRT, A., FUNICIELLO, R., AND TORTORICI, L., 2004a, Quaternary deformation pattern in a hinterland, foredeep to foreland system deduced by AMS, Structural and Paleomagnetic data: the example of eastern Sicily: Journal of Structural Geology, v. 26, p. 29–46.

CIFELLI, F., MATTEI, M., HIRT, A.M., AND GUNTHER, A., 2004b, The origin of tectonic fabrics in ''undeformed'' clays: the early stages of deformation in extensional sedimentary basins: Geophysical Research Letters, v. 31, no. L09604, doi: 10.1029/2004GL019609.

CIFELLI, F., MATTEI, M., CHADIMA, M., HIRT, A.M., AND HANSEN, A., 2005, The origin of the tectonic lineation in extensional basins: combined neutron texture and magnetic analysis on ''undeformed'' clays: Earth and Planetary Science Letters, v. 235, p. 62–78.

CIFELLI, F., MATTEI, M., CHADIMA, M., LENSER, S., AND HIRT, A.M., 2009, The magnetic fabric in ''undeformed clays'': AMS and neutron texture analyses from the Rif Chain (Morocco): Tectonophysics, v. 466, p. 79–88.

COSTA, E., PIALLI, G., AND PLESI, G., 1998, Foreland basins of the Northern Apennines; relationships with passive subduction of the Adriatic lithosphere: Società Geologica Italiana, Memorie, v. 52, p. 595–606.

COLLINSON, J.D., AND THOMPSON, D.B., 1982, Sedimentary Structures: London, George Allen and Unwin, 194 p.

COLWELL, J.B., AND EXON, N.F., 1988, Quaternary hemipelagic sedimentation in the basins flanking the Solomon Islands volcanic arc: Geo-Marine Letters, v. 8, p. 139–147.

DENNIELOU, B., 1997, Dynamique sédimentaire sur le plateau des Açores pour les derniers 400 ka: Thèse de doctorat, Université de Bretagne Occidentale, 341 p.

DONDI, L., MOSTARDINI, F., AND RIZZINI, A., 1982, Evoluzione sedimentaria e paleogeografica nella Pianura Padana, *in* Guida alla Geologia del Margine Appenninico–Padano: Società Geologica Italiana, p. 47–58.

ELLWOOD, B.B., 1980, Induced and remanent magnetic properties of marine sediments as indicators of depositional processes: Marine Geology, v. 38, p. 233–244.

ESCUTIA, C., EITTREIM, S.L., COOPER, A.K., AND NELSON, C.H., 2000, Morphology and acoustic character of the Antarctic Wilkes Land turbidite systems: ice-sheets-sourced versus river-sourced fans: Journal of Sedimentary Research, v. 70, p. 84–93.

FELLETTI, F., 2004, Statistical modelling and validation of correlation in turbidites: an example from the Tertiary Piedmont Basin (Castagnola Fm., North Italy): Marine and Petroleum Geology, v. 21, p. 23–39.

FELLETTI, F., AND BERSEZIO, R., 2010a, Quantification of the degree of confinement of a turbidite-filled basin: a statistical approach based on bed thickness distribution: Marine and Petroleum Geology, v. 27, p. 515–532.

FELLETTI, F., AND BERSEZIO, R., 2010b, Validation of Hurst statistics: a predictive tool to discriminate turbiditic sub-environments in a confined basin: Petroleum Geoscience, v. 16, p. 401–412.

FELLETTI, F., CARRUBA, S., AND CASNEDI, R., 2009, Sustained turbidity currents: evidence from the Pliocene Periadriatic foredeep (Cellino Basin, Central Italy), *in* Kneller, B., Martinsen, O.J., and McCaffrey, B., eds., External Controls on Deep-Water Depositional Systems: SEPM, Special Publication 92, p. 325–346.

FISHER, R.A., 1953, Dispersion on a sphere: Royal Society of London, Proceedings, Series A, v. 217, p. 295–305.

GANDOLFI, G., PAGANELLI, L., AND ZUFFA, G.G., 1983, Petrology and dispersal pattern (Miocene, Northern Apennines): Journal of Sedimentary Petrology, v. 53, p. 493–507.

GONTHIER, E.G., FAUGERES, J.C., AND STOW, D.A.V., 1984, Contourite facies of the Faro drift, Gulf of Cadiz, *in* Stow, D.A.V., and Piper, D.J.W., eds., 1984, Fine Grained Sediments; Deep-Water Processes and Facies, Geological Society of London, Special Publication 15, p. 275–292.

HAMILTON, N., AND REES, A.I., 1970, The use of magnetic fabric in paleocurrent estimation *in* Runcorn, S.K., ed., 1970, Palaeogeophysics: New York, Academic Press, p. 445–464.

←

FIG. 5.—Stereographic projection of principal axes of magnetic susceptibility (k_{max} = squares, k_{int} = triangles, k_{min} = circles) for the entire WM beds dataset (N = geographic north; sites = number of sites; n = number of samples) plotted in **A)** *in situ* and **B)** tilt-corrected coordinates. **C)** Rose diagram showing in black the preferred k_{max} orientation of the entire WM beds dataset in tilt-corrected coordinates; a general northwest–southeast trend (without correction for Apennine thrust-sheet rotation) is clearly evident. The same preferred k_{max} orientation corrected for Apennine thrust-sheet rotation of 29 ± 8° counterclockwise since the Oligo-Miocene (Speranza et al. 1997) is indicated in gray. **D)** Plot of the shape parameter T versus the corrected anisotropy degree P_j for the studied samples. **E)** Flinn-type plot of the studied samples (L = magnetic lineation; F = magnetic foliation); see Table 2 for data.

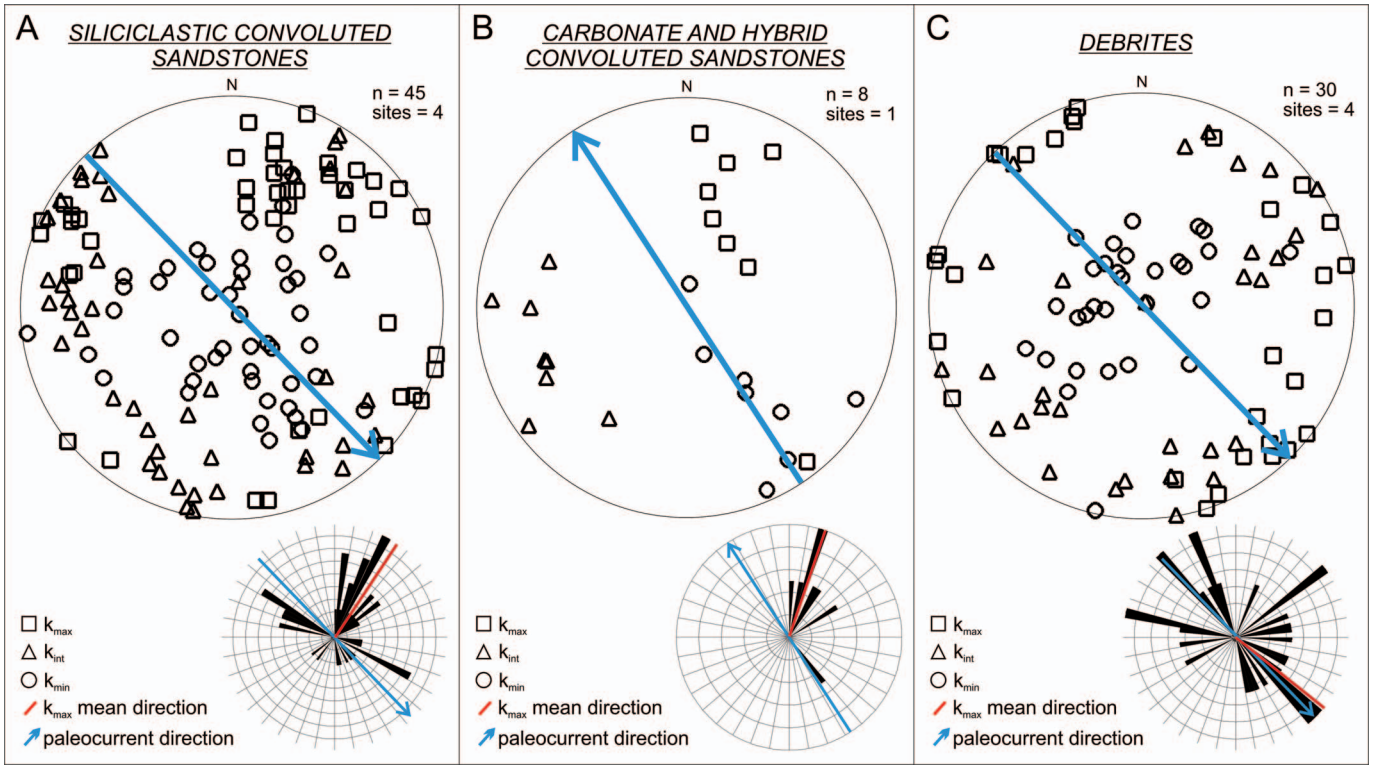

FIG. 7.—Stereographic projection of principal axes of magnetic susceptibility (k_{max} = squares, k_{int} = triangles, k_{min} = circles) plotted in tilt-corrected coordinates, and rose diagram showing the mean direction of the k_{max} (N = geographic north; sites = number of sites; n = number of samples) of **A)** siliciclastic convoluted sandstones, **B)** carbonate and hybrid convoluted sandstones, and **C)** debrites. These sediments show a very high dispersion of the susceptibility axes due to sedimentological processes, e.g., dewatering (see text for discussion).

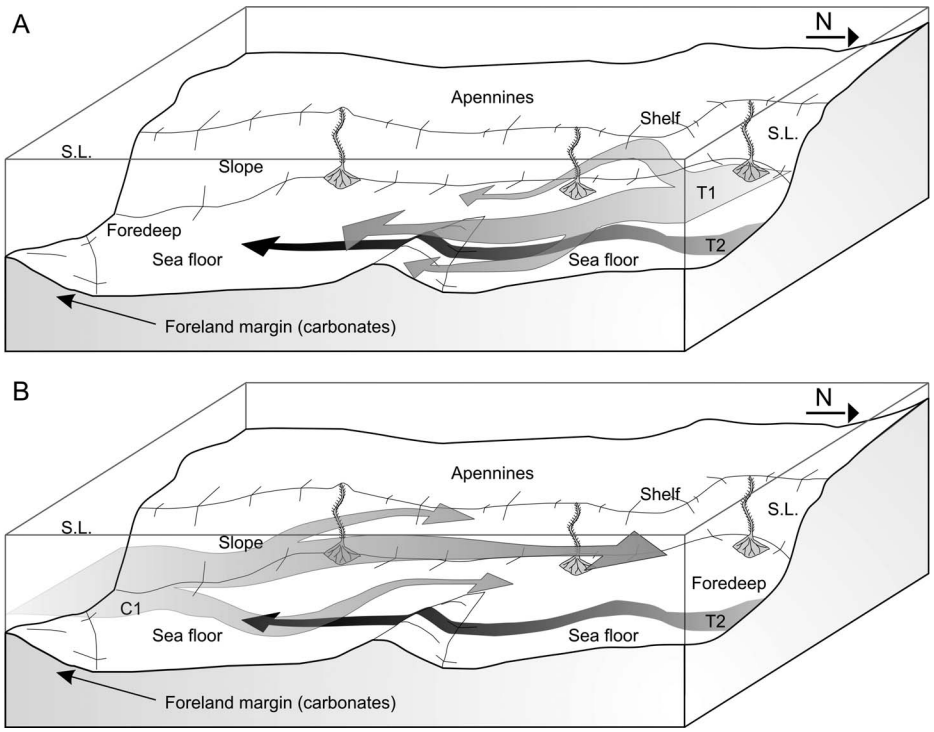

FIG. 8.—Alternative mechanisms to explain the WM beds. **A)** The WM beds could have been deposited from an essentially stationary suspension cloud (T1) that is produced from a fading turbidity current (T2), implying that the WM beds resulted from hydraulic sorting of the finer and lighter particles (e.g., carbonates, phyllosilicates) toward the upper part of the flow, and constitute the distal end members of a turbiditic facies tract (end of Bouma's T_e division). **B)** Preferentially, the WM beds could represent muddy contourites deposited from semipermanent bottom currents (C1) flowing parallel to the basin axis, which is our preferred option as discussed in the text. (S.L. = sea level; N = geographic north). See text for discussion.

Harms, J.C., Southard, J.B., and Walker, R.G., 1982, Structures and Sequences in Clastic Rocks: SEPM, Short Course 9, 249 p.

Hendry, H.E., 1976, The orientation of discoidal clasts in resedimented conglomerates, Cambro-Ordovician, Gaspé, eastern Quebec: Journal of Sedimentary Petrology, v. 46, p. 48–55.

Hesse, R., 1975, Turbiditic and non-turbiditic mudstone of Cretaceous flysch sections of the East Alps and other basins: Sedimentology, v. 22, p. 387–416.

Housen, B., van der Pluijm, B.A., and Essene, E.J., 1995, Plastic behavior of magnetite and high strains obtained from magnetic fabrics in the Parry Sound shear zone, Ontario Grenville Province: Journal of Structural Geology, v. 17, p. 265–278.

Howe, J.A., 1995, Sedimentary processes and variations in slope current activity during the last glacial–interglacial episode on the Hebrides Slope, Northern Rockall Trough, North Atlantic Ocean: Sedimentary Geology, v. 96, p. 201–230.

Howe, J.A., 1996, Turbidite and contourite sediment waves in the northern Rockall Trough, North Atlantic Ocean: Sedimentology, v. 43, p. 219–234.

Hrouda, F., 1982, Magnetic anisotropy of rocks and its application in geology and geophysics: Surveys in Geophysics, v. 5, p. 37–82.

Jelinek, V., 1978, Statistical processing of anisotropy of magnetic susceptibility measured on groups of specimens: Studia Geophysica et Geodaetica, v. 22, p. 50–62.

Jelinek, V., 1981, Characterization of the magnetic fabric of rocks: Tectonophyics, v. 79, p. 63–67.

Johansson, C.E., 1964, Orientation of pebbles in running water: a laboratory study: Geografiska Annaler, v. 45, p. 85–112.

Kissel, C., Barrier, E., Laj, C., and Lee, T.Q., 1986, Magnetic fabric in "underformed" marine clays from compressional zones: Tectonics, v. 5, p. 769–781.

Knutz, P.C., Jones, E.J.W., Austin, W.E.N., and van Weering, T.C.E., 2002, Glacimarine slope sedimentation, contourite drifts and bottom current pathways on the Barra Fan, UK North Atlantic margin: Marine Geology, v. 188, p. 129–146.

Kuenen, P.H., 1964, Deep-sea sands and ancient turbidites, *in* Bouma, A.H., and Brouwer, A., eds., Turbidites: Amsterdam, Elsevier, p. 3–33.

Lowrie, W., 1990, Identification of ferromagnetic minerals in a rock by coercivity and unblocking temperature properties: Geophysical Research Letters, v. 17, p. 159–162.

Lowrie, W., and Hirt, A.M., 1987, Anisotropy of magnetic susceptibility in the Scaglia Rossa pelagic limestone: Earth and Planetary Science Letters, v. 82, p. 349–356.

Mattei, M., Funicello, R., and Kissel, C., 1995, Paleomagnetic and structural evidence for Neogene block rotations in the Central Apennines, Italy: Journal of Geophysical Research, v. 100, p. 17863–17883.

McBride, E., and Picard, D., 1991, Facies implications of *Trichichnus* and *Chondrites* in turbidites and hemipelagites, Marnoso-Arenacea Formation (Miocene), northern Apennines, Italy: Palaios, v. 6, p. 281–290.

Monaco, P., 2008, Taphonomic features of *Paleodictyon* and other graphoglyptid trace fossils in Oligo-Miocene thin-bedded turbidites, northern Apennines, Italy: Palaios, v. 23, p. 667–682.

Monaco, P., and Checconi, A., 2008, Stratinomic indications by trace fossils in Eocene to Miocene turbidites and hemipelagites of the Northern Apennines (Italy): Studi Trentini di Scienze Naturali, Acta Geologica, v. 83, p. 133–163.

Mulder, T., Faugères, J.C., and Gonthier, E., 2008, Mixed turbidite–contourite systems, *in* Rebesco, M., and Camerlenghi, A., eds., Contourites: Amsterdam, Elsevier, Developments in Sedimentology, v. 60, p. 435–456.

Mulder, T., Zaragosi, S., Razin, P., Grelaud, C., Lanfumey, V., and Bavoil, F., 2009, A new conceptual model for the deposition process of homogenite; application to a Cretaceous megaturbidite of the western Pyrenees (Basque region, SW France): Sedimentary Geology, v. 222, p. 263–273.

Mutti, E., 1977, Distinctive thin-bedded turbidite facies and related depositional environments in the Eocene Hecho Group (South-Central Pyrenees, Spain): Sedimentology, v. 24, p. 107–131.

Mutti, E., 1979, Turbidites et cones sous-marins profonds, *in* Homewood, P., ed., Sédimentation Détritique (Fluviatile, Littorale et Marine): Université de Fribourg, Institut de Géologie, p. 353–419.

Mutti, E., and Johns, D.R., 1979, The role of sedimentary by-passing in the genesis of basin plain and fan fringe turbidites in the Hecho Group System (South-Central Pyrenees): Società Geologica Italiana, Memorie, v. 18, p. 15–22.

Mutti, E., and Ricchi Lucchi, F., 1972, Le torbiditi dell'Apennino settentrionale: introduzione all'analisi di facies: Società Geologica Italiana, Memorie, v. 11, p. 161–199.

Mutti, E., Ricchi Lucchi, F., 1975, Field Trip A-11: Turbidite facies and facies associations, *in* Mutti, E., Parea, G.C., Ricci Lucchi, F., Sagri, M., Zanzucchi, G., Ghibaudo, G., and Iaccarino, I., eds., Examples of Turbidite Facies Associations from Selected Formations of Northern Apennines: International Association of Sedimentologists, 9th International Congress, Nice, France, p. 21–36.

Mutti, E., Ricci Lucchi, F., and Roveri, M., 2002, Revisiting Turbidites of the Marnoso-Arenacea Formation and their Basin-Margin Equivalents: Problems with Classic Models, Excursion Guidebook: Workshop organized by Dipartimento di Scienze della Terra (Universita' di Parma) and Eni-Divisione Agip, 64th EAGE Conference and Exhibition, Florence, Italy, May 27–30, 120 p.

Muttoni, G., Argnani, A., Kent, D.V., Abrahamsen, N., and Cibin, U., 1998, Paleomagnetic evidence for Neogene tectonic rotations in the Northern Appennines, Italy: Earth and Planetary Science Letters, v. 154, p. 25–40.

Muttoni, G., Argnani, A., Ken, D.V., Abrahamsen, N., and Cibin, U., 2000, Paleomagnetic evidence for a Neogene two-phase counterclockwise tectonic rotation in the Northern Apennines (Italy): Tectonophysics, v. 326, p. 241–253.

Muzzi Magalhaes, P., and Tinterri, R., 2010, Stratigraphy and depositional setting of slurry and contained (reflected) beds in the Marnoso-Arenacea Formation (Langhian–Serravallian) Northern Apennines, Italy: Sedimentology, v. 57, p. 1685–1720.

Normark, W.R., and Piper, D.J.W., 1972, Sediments and growth pattern of Navy deep-sea fan, San Clemente Basin, California borderland: The Journal of Geology, v. 80, p. 198–223.

Park, M.H., Kim, J.H., Ryu, B.J., Kim, I.S., and Chang, H.W., 2006, AMS radiocarbon dating of the marine late Pleistocene–Holocene sediment cores from the western Ulleung Basin, East/Japan Sea. Nuclear Instruments and Methods in Physics Research, Section B: Beam Interactions with Materials and Atoms, v. 243, p. 211–215.

Parés, J.M., and Dinarès-Turell, J., 1993, Magnetic fabric in two sedimentary rock types from the Southern Pyrenees: Journal of Geomagnetism and Geoelectricity, v. 45, p. 193–205.

Parés, J.M., van der Pluijm, B.A., and Dinarès-Turell, J., 1999 Evolution of magnetic fabrics during incipient deformation of mudrocks (Pyrenees, northern Spain): Tectonophysics, v. 307, p. 1–14.

Parés, J.M., Hassold, N.J.C., Rea, D.K., and van der Pluijm , B.A., 2007, Paleocurrent directions from paleomagnetic reorientation of magnetic fabrics in deep-sea sediments at the Antarctic Peninsula Pacific margin (ODP Sites 1095, 1101): Marine Geology, v. 242, p. 261–269.

Pettijohn, F.J., 1975, Sedimentary Rocks, Third Edition: New York, Harper and Row Publishers, 628 p.

Piper, D.J.W., 1978, Turbidite muds and silts on deepsea fans and abyssal plains, *in* Stanley, D.J., and Kelling, G., eds., Sedimentation in Submarine Canyons, Fans and Trenches: Stroudsburg, Pennsylvania, Dowden, Hutchinson and Ross, p. 163–176.

Pudsey, C.J., 2000, Sedimentation on the continental rise west of the Antarctic Peninsula over the last three glacial cycles: Marine Geology, v. 167, p. 313–338.

Rebesco, M., and Camerlenghi, A., 2008, Contourites: Amsterdam, Elsevier, Developments in Sedimentology 60, 663 p.

Rebesco, M., Larter, R.D., Camerlenghi, A., and Barker, P.F., 1996, Giant sediment drifts on the continental rise west of the Antarctic Peninsula: Geo-Marine Letters, v. 16, p. 65–75.

Rebesco, M., Larter, R.D., Barker, P.F., Camerlenghi, A., and Vanneste, L.E., 1997, The history of sedimentation on the continental rise west of the Antarctic Peninsula: American Geophysical Union, Geology and Seismic Stratigraphy of the Antarctic Margin, Part 2, Antarctic Research Series, v. 71, p. 29–49.

Reeder, M.S., Rothwell, G., and Stow, D.A.V., 2002, The Sicilian gateway: anatomy of the deep-water connection between East and West Mediterranean basins, *in* Stow, D.A.V., Pudsey, C.J., Howe J.A, and Viana, A.R., eds., Deep-Water Contourite Systems: Modern Drifts and Ancient Series, Seismic and Sedimentary Characteristics: Geological Society of London, Memoir 22, p. 171–190.

Remacha, E., Fernández, L.P., and Maestro, E., 2005, The transition between sheet-like lobe and basin-plain turbidites in the Hecho Basin (South-Central Pyrenees, Spain): Journal of Sedimentary Research, v. 75, p. 798–819.

Ricci Lucchi, F., 1969, Recherches stratonomiques et sédimentologiques sur le Flysch Miocène de la Romagna (Formation Marnoso–Arenacea): Proceedings of the IV Session Committee on Mediterranean Neogene Stratigraphy, Giornale di Geologia, v. 36, p. 163–198.

Ricci Lucchi, F., 1975, Depositional cycles in two turbidite formations of northern Apennines (Italy): Journal of Sedimentary Petrology, v. 45, p. 3–43.

Ricci Lucchi, F., 1978, Turbidite dispersal in a Miocene deep-sea plain: Geologie en Mijnbouw, v. 57, p. 559–576.

Ricci Lucchi, F., 1979, Ricostruzione geometrica parziale di un lobo di conoide sottomarina: Società Geologica Italiana, Memorie, v. 18, p. 125–133.

Ricci Lucchi, F., 1981, The Marnoso arenacea turbidites, Romagna and Umbria Apennines, *in* Ricci Lucchi, F., ed., Excursion Guidebook, with Contribution on Sedimentology of Some Italian Basins, International Association of Sedimentologists, 2nd European Meeting, Bologna, p. 229–303.

Ricci Lucchi, F., 1986, The Oligocene to Recent foreland basins of the Northern Apennines, *in* Allen, P.A., and Homewood, P., eds., Foreland Basins: International Association of Sedimentologists, Special Publication 8, p. 105–139.

Ricci Lucchi, F., and Valmori, E., 1980, Basin-wide turbidites in a Miocene, over-supplied deep-sea plain: a geometrical analysis: Sedimentology, v. 27, p. 241–270.

Rupke, N.A., 1975, Deposition of fine-grained sediments in the abyssal environment of the Algero–Balearic Basin, western Mediterranean Sea: Sedimentology, v. 22, p. 95–109.

Sagnotti, L., and Meloni, A., 1993, Pleistocene rotations and strain in southern Italy: the example of the Sant'Arcangelo Basin: Annali di Geofisica, v. 36, p. 83–95.

Sagnotti, L., and Speranza, F., 1993, Magnetic fabric analysis of the Plio–Pleistocene clayey units of the Sant'Arcangelo basin, southern Italy: Physics of the Earth and Planetary Interiors, v. 77, p. 165–176.

Schwarzacher, W., 1963, Orientation of crinoids by current action: Journal of Sedimentary Petrology, v. 33, p. 580–586.

Shor, A.N., Kent, D.V., and Flood, R.D., 1984, Contourite or turbidite? Magnetic fabric of fine-grained Quaternary sediments, Nova Scotia continental rise, *in* Stow, D.A.V., and Piper D.J.W., eds., Fine-Grained Sediments; Deep-Water Processes and Facies: Geological Society of London, Special Publication 15, p. 257–273.

Speranza, F., Sagnotti, L., and Mattei, M., 1997, Tectonics of the Umbria–Marche–Romagna arc (central-northern Apennines, Italy): new paleomagnetic constraints: Journal of Geophysical Research, v. 102, p. 3153–3166.

Stacey, F.D., Joplin, G., and Lindsay, J., 1960, Magnetic anisotropy and fabric of some foliated rocks from SE Australia: Geofisica Pura e Applicata, v. 47, p. 30–40.

Stanley, D.J., 1988, Turbidities reworked by bottom currents: Upper Cretaceous examples from St. Croix, US Virgin Islands: Smithsonian Contributions to Marine Science, v. 33, 79 p.

Stow, D.A.V., 1982, Bottom currents and contourites in the North Atlantic: Institut de Géologie du Bassin d'Aquitaine, Bulletin, v. 31, p. 151–166.

Stow, D.A.V., and Faugères, J.C., 2008, Contourites facies and facies model, *in* Rebesco, M., and Camerlenghi, A., eds., Contourites, Amsterdam, Elsevier, Developments in Sedimentology, v. 60, p. 223–250.

Stow, D.A.V., and Lovell, J.P.B., 1979, Contourites: their recognition in modern and ancient sediments: Earth-Science Reviews, v. 14, p. 251–291.

Stow, D.A.V., and Piper, D.J.W., 1984, Fine-Grained Sediments; Deep-Water Processes and Facies: Geological Society of London, Special Publication 15, 659 p.

Stow, D.A.V., and Tabrez, A.R., 1998, Hemipelagites: processes, facies and model, *in* Stoker, M.S., Evans, D., and Cramp, A., eds., Geological Processes on Continental Margins: Geological Society of London, Special Publication 129, p. 317–337.

Stow, D.A.V., and Wetzel, A., 1990, Hemiturbidite: a new type of deep-water sediment, *in* Cochran, J.R., and Stow, D.A.V., eds., Proceedings of the Ocean Drilling Program, Scientific Results: College Station, Texas, U.S.A., v. 116, p. 25–34.

Stow, D.A.V., Wezel, F.C., Savelli, D., Rainey, S.R.C., and Angell, G., 1984, Depositional model for calcilutites: Scaglia Rossa limestones, Umbro–Marchean Apennines, *in* Stow, D.A.V., and Piper, D.J.W., eds., Fine-Grained Sediments; Deep-Water Processes and Facies: Geological Society of London, Special Publication 15, p. 223–241.

Stow, D.A.V., Faugères, J.C., Viana, A.R., and Gonthier, E., 1998, Fossil contourites; a critical review: Sedimentary Geology, v. 115, p. 3–31.

Stow, D.A.V., Hernandez-Molina, F.J., Llave, E., Sayago-Gil, M., Diaz del Rio, V., and Branson, A., 2009, Bedform velocity matrix: the estimation of bottom current velocity from bedform observations: Geology, v. 37, p. 327–330.

Taira, A., 1989, Magnetic fabric and depositional processes, *in* Taira, A., and Masuda, F., eds., Sedimentary Facies in the Active Plate Margin: Tokyo, Terra Science Publication, p. 44–77.

Taira, A., and Scholle, P.A., 1979, Deposition of resedimented sandstone beds in the Pico Formation, Ventura Basin, California, as interpreted from magnetic fabric measurements: Geological Society of America, Bulletin, v. 90, p. 952–962.

Talling, P.J., 2001, On the frequency distribution of turbidite thickness: Sedimentology, v. 48, p. 1297–1329.

Talling, P.J., Amy, L.A., Wynn, R.B., Blackbourn, G., and Gibson, O., 2007, Evolution of turbidity currents deduced from extensive thin turbidites: Marnoso Arenacea Formation (Miocene), Italian Apennines: Journal of Sedimentary Research, v. 77, p. 172–196.

Talling, P.J., Malgesini, G., Sumner, E.J., Amy, L.A., Felletti, F., Blackbourn, G., Nutt, C., Wilcox, C., Harding, I.C., and Akbari, S., 2012a, Planform geometry, stacking pattern, and extrabasinal origin of low strength and intermediate strength cohesive debris flow deposits in the Marnoso-Arenacea Formation, Italy: Geosphere, v. 8, p. 1–24, doi: 10.1130/GES00734.1.

Talling, P.J., Malgesini, G., and Felletti, F., 2012b, Can liquefied debris flows deposit clean sandstone over large areas of sea floor? Field evidence from the Marnoso-Arenacea Formation, Italian Apennines: Sedimentology, doi: 10.1111/j.1365-3091.2012.01358.x.

Tarling, D.H., and Hrouda, F., 1993, The Magnetic Anisotropy of Rocks: London, Chapman and Hall, 212 p.

Vai, G.B., 2001, GSSP, IUGS and IGC: an endless story toward a common language in the earth sciences: Episodes, v. 24, p. 29–31.

Van der Pluijm, G.J., 1969, The turbidite problem: New Zealand Journal of Geology and Geophysics, v. 12, p. 7–50.

Viana, A.R. 2008, Economic relevance of Conturites, *in* Rebesco, M., and Camerlenghi, A., eds., Contourites: Amsterdam, Elsevier, Developments in Sedimentology 60, p. 493–510.

Received 1 July 2011; accepted 17 September 2012.